2D Materials

RECEIVED
24 February 2020

ACCEPTED FOR PUBLICATION
9 March 2020

PUBLISHED
28 April 2020

PAPER

Crystal structure reconstruction in the surface monolayer of the quantum spin liquid candidate α-$RuCl_3$

Zhongwei Dai[1], Jie-Xiang Yu[2,3], Boyi Zhou[4,8], Samuel A Tenney[1], Paula Lampen-Kelley[5,6], Jiaqiang Yan[5,6], David Mandrus[5,6], Erik A Henriksen[4,7], Jiadong Zang[2], Karsten Pohl[2] and Jerzy T Sadowski[1,9]

[1] Center for Functional Nanomaterials, Brookhaven National Laboratory, Upton, New York 11973, United States of America
[2] Department of Physics and Astronomy and Materials Science Program, University of New Hampshire, Durham, New Hampshire 03824, United States of America
[3] Center for Molecular Magnetic Quantum Materials, University of Florida, Gainesville, Florida 32611, United States of America
[4] Department of Physics, Washington University in St. Louis, MO 63130, United States of America
[5] Materials Science and Technology Division, Oak Ridge National Laboratory, Oak Ridge, Tennessee 37831, United States of America
[6] Department of Materials Science and Engineering, University of Tennessee, Knoxville, Tennessee 37996, United States of America
[7] Institute for Materials Science and Engineering, Washington University in St. Louis, MO 63130, United States of America

E-mail: sadowski@bnl.gov

Keywords: $RuCl_3$, low-energy electron diffraction, dynamical LEED analysis, surface structure, surface buckling

Abstract

α-$RuCl_3$, a layered 2D material, was recently identified as a promising candidate for realizing a Kitaev quantum spin liquid. However one fundamental property, the crystal structure, has not been well resolved yet due to difficulty of bulk diffraction techniques caused by layer stacking faults. Furthermore, the surface relaxation of monolayer-level thin films is completely unknown yet. In this report, surface sensitive low energy electron diffraction technique with μm selectivity (μ-LEED) combined with dynamical LEED analysis were used to reveal the detailed crystal structure of the surface monolayer of α-$RuCl_3$. A surface structural distortion that breaks the inversion symmetry of the ideal bulk structure was revealed. To be specific, we found the surface Cl sub-lattice is buckled with one Cl atom approximately 0.16 Å below the other two Cl atoms, in the unit cell. The Ru atomic layer shows an even larger buckling of approximately 0.31 Å. Through density functional theory (DFT) calculations, we suggested that this surface distortion may be induced by Cl-vacancies that are inevitable in this material system. Inversion symmetry breaking in this material could have a significant impact on the 2D Kitaev interaction for both, interfaces with other 2D materials, such as graphene and future monolayer devices.

1. Introduction

The quantum spin liquid state (QSLs) is a recently proposed third ground state of quantum magnet [1–4]. Unlike the known anti-ferromagnetic (AFM) and ferromagnetic (FM) states, the spins in the QSLs do not order in the ground state, but exhibit long-range quantum entanglement [3]. Finding experimental evidence of the QSLs in real materials has been a long-sought goal in condensed matter physics. The QSLs is considered to play an important role in various physics phenomena, such as superconductivity [4] and long-range spin entanglement [5]. Particularly the possible presence of Majorana fermions therein could be the building block of quantum computing [6, 7]. Among various QSLs models, Kitaev has proposed a two-dimensional (2D) honeycomb model which is exactly solvable [8]. It thus becomes an ideal test bed for understanding related phenomena. Real materials systems that can host a Kitaev QSL are rare and need to fulfill two key factors: *(i)* Magnetic atoms carrying effective spin-1/2 on a 2D honeycomb lattice and *(ii)* strong spin-orbital coupling which induces anisotropic bond-dependent spin-spin interaction. Inherent to its nature, the spin-spin interactions in Kitaev's model are sensitive to the lattice structure and bond-length [9]. Previously, iridates [10–13], such as Na_2IrO_3, had been identified as one of the most promising candidates for hosting a Kitaev QSLs.

[8] Current address: Department of Physics and Astronomy, Purdue University, West Lafayette, Indiana, 47 907
[9] Corresponding author: sadowski@bnl.gov

However, it was later discovered that Na_2IrO_3 has a small unit-cell distortion [13] and surface crystal structure reconstruction [14] which has raised questions for its applicability of Kitaev physics [15, 16]. In the mean time, α-$RuCl_3$, a layered van der Waals material, has emerged as another viable candidate. Each single-layer of α-$RuCl_3$ consists of a covalently-bonded Cl-Ru-Cl sandwich of atomic layers, with thickness $w = 2.657$ Å, as shown in figure 1(b). Monolayer α-$RuCl_3$ was considered to approximate Kitaev's crystal structure model, with Ru atoms, forming a 2D honeycomb lattice, carrying effective spin-1/2 moment. Due to spin-orbital coupling, nearest-neighbor spins experience anisotropic spin-spin exchange interactions parameterized by J_x, J_y and J_z [17]. Each individual Cl-Ru-Cl sandwich layer is weakly bonded to neighboring layers by van der Waals force, with interlayer spacing $d = 3.021$ Å, as shown in figure 1(b). The interlayer magnetic interaction was estimated to be rather weak which makes the structure of α-$RuCl_3$ a very good approximation of Kitaev's pure 2D model [17]. Several recent reports, including inelastic neutron scattering [17, 18] and quantum thermal Hall effect measurements [6], provided some indirect but exciting evidence to support Kitaev QSLs in α-$RuCl_3$. However, one of the fundamental properties, the crystal structure, is still under debate [9, 17, 19]. Banerjee *et al* concluded that α-$RuCl_3$ has a crystal structure of symmetry group $P3_112$, with a three-fold rotational symmetry in-plane and ABC layer stacking in the out-of-plane direction [17], as shown in figure 1. On the other hand, Johnson *et al* concluded that α-$RuCl_3$ should be of symmetry group *C2/m*, which is monoclinic with one layer in the unit cell [14]. Even though their conclusions are different, both noted that the difference between the $P3_112$ and *C2/m* structure models are very small and could not be easily differentiated experimentally due to potential layer stacking fault. Furthermore, current electronic properties studies by angle-resolved photoemission spectroscopy (ARPES) have been hindered by poor agreement between theory and the measured band structure [20, 21], probably due to lack of accurate input of intra-layer atomic structure. A more detailed experimental investigation in the intra-layer atomic structure of individual Cl-Ru-Cl sandwich layer is therefore needed. Due to weak inter-layer bonding, α-$RuCl_3$ can be mechanically exfoliated down to a monolayer [22, 23], which is a closer realization of Kitaev's 2D model. Exfoliated 2D systems are also useful for fabricating prototype devices for exploring applications in quantum computing. Recently, peculiar transport properties have been reported on heterostructure device of graphene on top of α-$RuCl_3$ [24, 25]. These reports revealed potentially strong interfacial interaction between the two dissimilar 2D materials. Detailed knowledge of the surface of α-$RuCl_3$ is needed for further understanding of the interface physics.

In this study, we utilize surface sensitive, non-intrusive low energy electron microscopy (LEEM) [26] and its complimentary *in situ* micro-spot surface diffraction (μ-LEED) [27–29] techniques to investigate the surface region of layered α-$RuCl_3$. We report the results of the first comprehensive LEED study of α-$RuCl_3$ and reveal the detailed crystal structure of the surface monolayer of exfoliated α-$RuCl_3$. The in-plane symmetry of the surface monolayer was first examined through diffraction pattern analysis. Furthermore, the detailed surface crystal structure was determined using dynamical LEED-*IV* analysis [28–31]. We find a surface symmetry breaking due to the unit-cell distortion of the crystal lattice, caused by the presence of surface defects. The interplay between lattice degree of freedom, vacancy defects and electronic spin and orbital is discussed.

2. LEEM and μ-LEED

α-$RuCl_3$ is a layered-structure material which can be exfoliated down to a single layer [22, 23]. Previous Raman studies on exfoliated α-$RuCl_3$ reported a symmetry-forbidden vibrational mode present in polarized Raman measurements [22]. The forbidden Raman mode is sensitive to both, temperature and sample thickness and is more prominent when the thickness is reduced. It was suspected that this Raman mode originates from a small surface layer crystal structure distortion [22]. In the present study, various α-$RuCl_3$ flakes were mechanically exfoliated onto an n-doped Si chip with native oxide, using a previously described method [32, 33] and then transferred to the low-energy electron microscope (LEEM) ultra-high vacuum (UHV) chamber (base pressure, 2×10^{-10} Torr), located at the Electron Spectro-Microscopy (ESM) beamline of the National Synchrotron Light Source II. The samples were then annealed at 573 K for an hour to remove adsorbates from the surface. Two types of samples were prepared and compared: *(i)* flakes exfoliated in air and *(ii)* flakes exfoliated in an inert Ar atmosphere in a glovebox and then transferred to the LEEM chamber without air exposure via a vacuum suitcase. The substrats were pre-patterned with fiducial gold marks, see figure 2 (a), the darker 'L-shape' feature, which allowed for easier location and characterization of the flakes of interest. Samples were first examined in real space using LEEM to find particular flakes. A LEEM image of an exfoliated α-$RuCl_3$ flake is shown in figure 2(a). Within the field of view, the brighter area is the exfoliated flake, the darker bar-like features within the brighter area are of different height compared to the rest of the flake, the dark area outside of the flake is the SiO_2 substrate. The flake shown in figure 2(a) is about 10 to 20 nm thick based on estimation by color contrast under an optical microscope. Subsequently, the selected-area LEED (μ-LEED) was conducted with 2 μm sampling

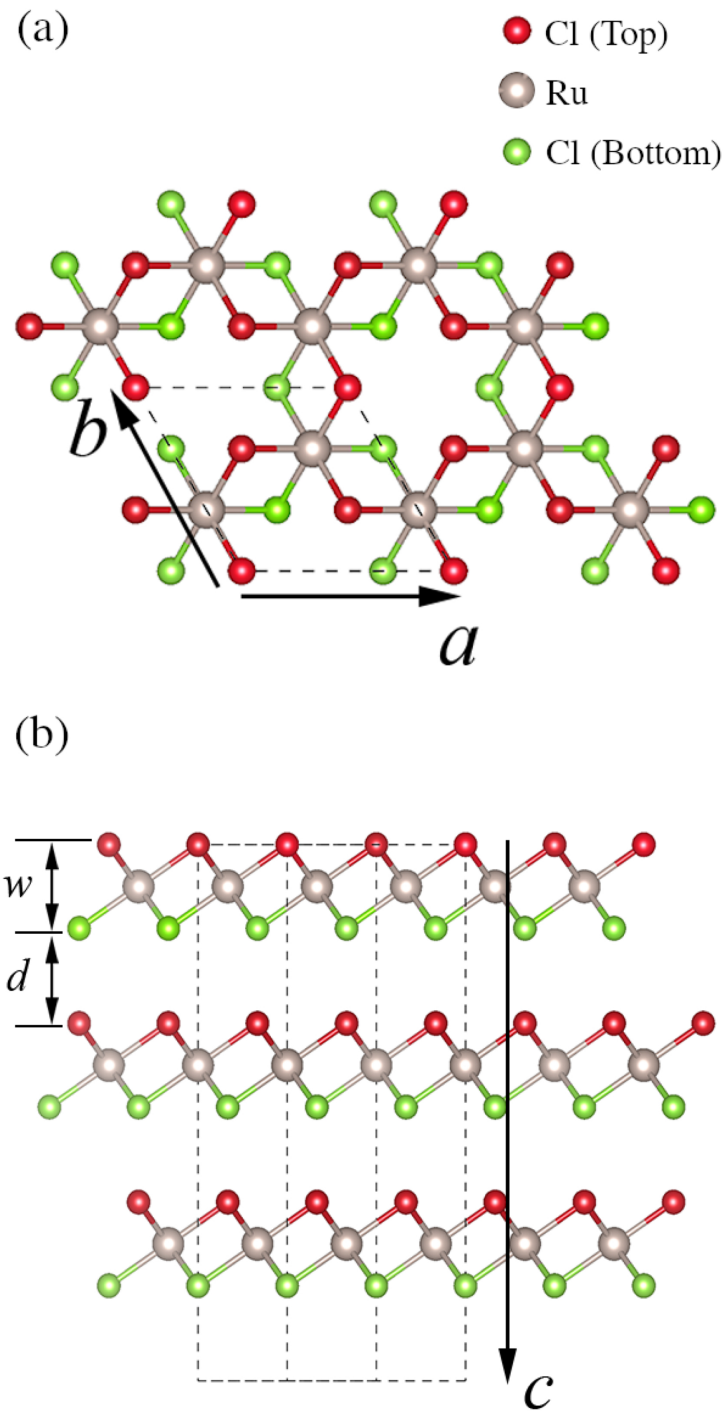

Figure 1. Crystal structure of α-$RuCl_3$, assuming $P3_112$ symmetry: (a) Top-view of single Cl-Ru-Cl sandwich layer, (b) Side-view of the bulk crystal unit cell, indicated by dashed line.

size to examine the surface crystallinity and in-plane symmetry. Due to the use of low-energy electrons in the μ-LEED experiments, we were able to examine only the surface monolayer of $RuCl_3$ and exclude the effects caused by layer stacking faults. The electron-mean-free-path is about 5–10 Å for the probing electrons of 35 to 150 eV. All LEEM and μ-LEED experiments were carried out in UHV at room temperature (RT). Figures 2(b) and (c) shows sharp diffraction patterns acquired at two different energies on the center area of the flake. The first important observation derived from diffraction patterns is their 3-fold symmetry which indicates the surface monolayer of α-$RuCl_3$ has an in-plane 3-fold rotational symmetry, at room temperature, as more clearly shown in figure 2(c), instead of 2-fold symmetry that Johnson *et al* proposed [9]. Both types of samples, exfoliated in air and exfoliated in the glovebox, show the same LEED pattern and same dynamical intensity response across the whole energy range probed. The diffraction beams are assigned to different groups (00), A, B and C, based on their intensity profile. Then they

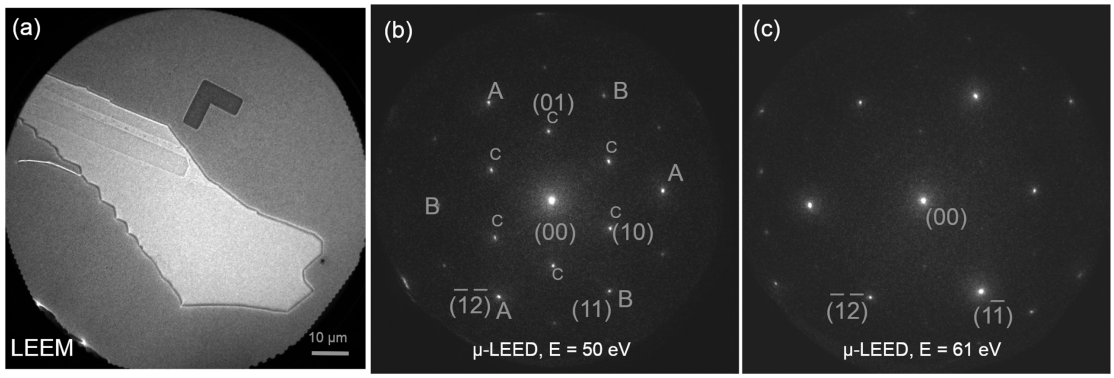

Figure 2. (a) LEEM (mirror mode) image of an exfoliated (~ 10 to 20 nm thick) α-$RuCl_3$ flake, field of view (FOV) is 100 μm; LEED pattern with incoming electron energy $E \approx 50$ eV (b), 61 eV (c), respectively.

are assigned Miller indices by comparing to diffraction pattern acquired on a well known Si(111)-7× 7 reconstructed surface [34, 35], under the same experimental settings. It was found that the C diffraction beams are first order diffraction beams, i.e. (01) or (10) beams, A and B are the second order beams, i.e. $(1\bar{1})$ and $(\bar{1}\bar{2})$, respectively. The intensities of C beams are much weaker (less than 10%), compared to the other beams. These weak diffraction spots, can be easily missed by conventional LEED [36]. This result is striking when looking more closely into the symmetry of the crystal lattice of single Cl-Ru-Cl sandwich layer. Based on the 3-fold symmetrical diffraction pattern observed and previous bulk diffraction results, undistorted single layer $RuCl_3$ should have an $\overline{R}_3$ symmetry, with an inversion symmetry point at the center of ruthenium atom honeycomb lattice. For structures with an $\overline{R}_3$ symmetry, only diffraction beams satisfying the following condition can be present: $h + k = 3 \cdot n$, where h and k are Miller indices and n is any integer. This means (01) and (10) diffraction spots should be absent, assuming perfect $\overline{R}_3$ symmetry. The same diffraction extinction rule was shown recently in a similar material in the transition-metal trihallides family, VI_3 [37]. However, our μ-LEED results are in direct contradiction to this expectation. The symmetry forbidden (10) and (01) diffraction spots are distinctively present in our observed LEED pattern, as shown in figure 2(b). The (01) and (10) spots are only visible when probed with electron beam energy within a small range around $E \approx 50$ eV. This can be understood since the probing electrons are the most sensitive to the surface structure at around 50 eV, based on the electron-mean-free-path universal curve [38]. The presence of (01) and (10) spots on the LEED pattern strongly indicates a symmetry breaking. Selected-area x-ray photoelectron spectroscopy (XPS) performed on flakes exfoliated in air confirmed a presence of oxygen in the surface layer, likely from adsorbed hydroxyls, while oxygen was not detected in the flakes exfoliated in a glovebox. However, exact same diffraction patterns were observed on all exfoliated $RuCl_3$ flakes, whether the exfoliation was performed in air, or in a glovebox, at temperatures ranging from RT up to 450 °C. Therefore we conclude that the observed symmetry breaking in the LEED pattern is not of ex-situ origin such as contamination of surface from air exposure. We believe the symmetry breaking is of intrinsic origin. Moreover, fractional order diffraction spots were not observed in any of the samples measured, thus we do not believe that surface reconstruction exists that would introduce a larger surface supercell. Instead, the observed symmetry breaking is likely caused by a slight lattice distortion in the surface monolayer of $RuCl_3$.

3. Dynamical μ-LEED-*IV* analysis

Dynamical LEED-*IV* analysis is a well established technique for surface crystal structure determination with sub-Å ngstrom precision [28–31]. Experimentally, diffraction patterns are acquired for a series of different incident electron energies, usually lower than 500 eV. The intensities of each one of the diffracted beams are extracted and plotted against the corresponding incoming electron energy. These curves are known as LEED-*IV* curves, as shown in figure 3. An initial atomic structural model is proposed based on observed LEED pattern and known bulk crystal structure. The model's atomic coordinates are input as parameters and multiple scattering theory with muffin-tin atomic potential model are used to calculate the LEED-*IV* curves [28, 29]. Calculated *IV* curves are compared to experimental curves. Through an iterative routine, atomic position coordinates are changed and optimized in order to achieve the best agreement with experiments. In the present study, we used calculation codes LEED*opt* from Adams [27], which were developed from the programs of Pendry [28] and Van Hove and Tong [29]. A χ^2-based reliability factor R_2 is used to quantify the difference between calculated and experimental *IV* curves [27]. The utilization of the R_2

Table 1. Optimized crystal structure of surface monolayer α-$RuCl_3$. '–' in Δ means the atom is moving closer to the surface.

	z_{Cl1} (Å)	z_{Cl2} (Å)	z_{Cl3} (Å)	z_{Ru1} (Å)	z_{Ru2} (Å)	z_{Cl4} (Å)	z_{Cl5} (Å)	z_{Cl6} (Å)	*R*-factor
Start Value (bulk structure)	0.000	0.000	0.000	1.328	1.328	2.657	2.657	2.657	0.23
Optimized	–0.106	0.062	–0.100	1.154	1.465	2.531	2.521	2.504	0.11
(Δ)	(–0.106)	(+0.062)	(–0.100)	(–0.174)	(+0.137)	(–0.126)	(–0.136)	(–0.153)	0.11

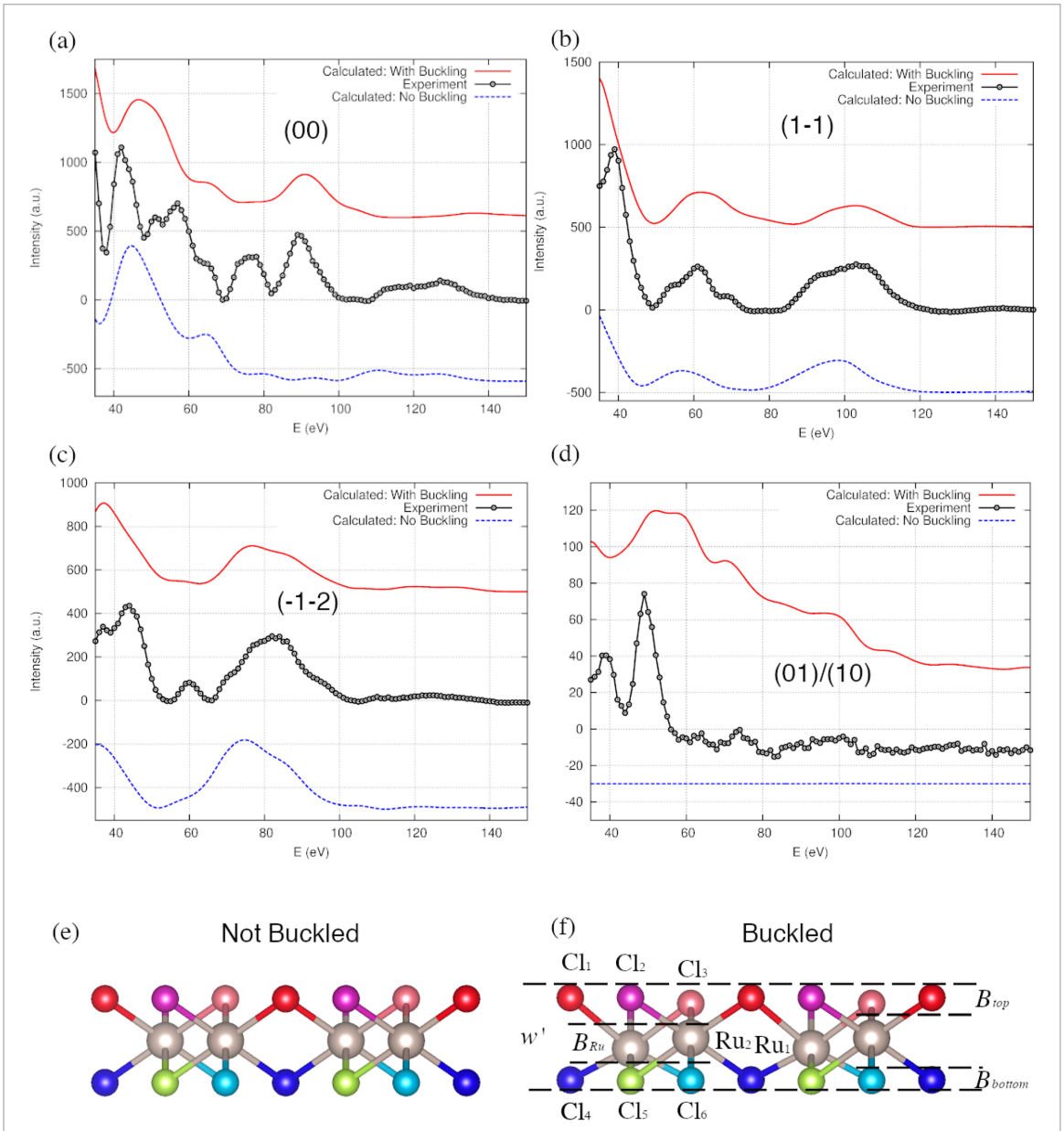

Figure 3. Comparison of calculated LEED-*IV* curves with optimized surface structural paratmeters (red) with experimental curves (black): (a) (00) beam; (b) $(1\bar{1})$ beam; (c) $(\bar{1}\bar{2})$ beam; (d) (01)/(10) beam. For comparison, the blue dashed lines in (a)–(d) are calculated LEED-*IV* curves assuming undistorted $\bar{R}_3$ symmetry, before structural optimization was performed. (e) Undistorted crystal structure of monolayer $RuCl_3$; (f) Optimized surface monolayer $RuCl_3$ crystal structure.

factor allows for the relative intensities of the diffraction beams to be preserved during the optimization, which enhances the reliability of the surface structure determination. The phase shifts (a quantity describing the atomic scattering property [29]) were calculated using the Barbieri/Van Hove phase shift calculation package [39]. The muffin-tin radii for Ruthenium and Chlorine atoms were set to r_{MT}^{Cl} = 1.878 a.u. and r_{MT}^{Ru} = 2.640 a.u., respectively and 12 phase shifts (L = 11) were used for the LEED-*IV* calculation. The in-plane lattice constants were set to $a = b = 5.963$ Å, the thickness of the Cl-Ru-Cl sandwich layer to $w = 2.657$ Å, and the interlayer distance to $d = 3.021$ Å for the bulk, as indicated in figure 1 [17]. The Debye temperature for Cl and Ru were set to $\theta_D^{Cl} = 205$ K and $\theta_D^{Ru} = 209$ K, respectively. The inner potential, $V_0 + iV_{im}$, was set to be independent of energy. The real part V_0 was initially set to 8 eV

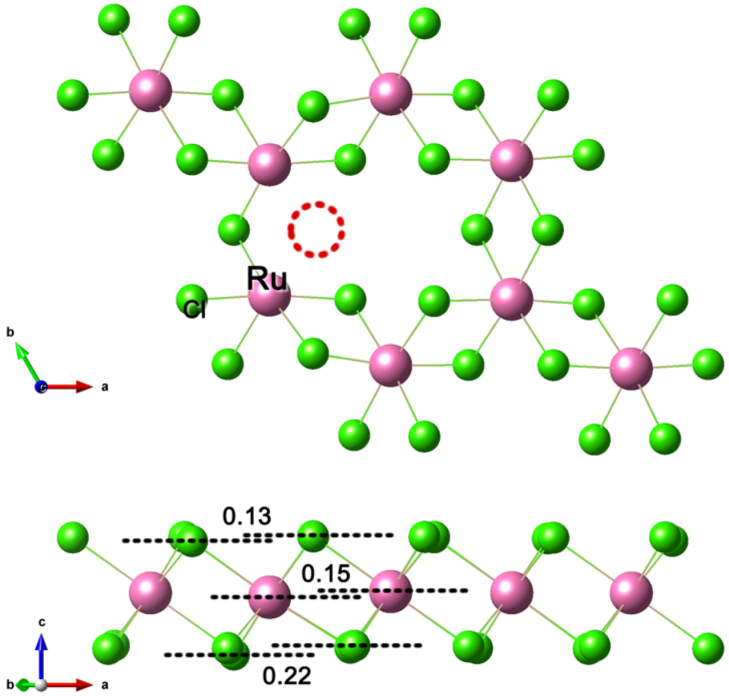

Figure 4. Top view (upper) and side view (lower) of 2× 2 supercell of one PL α-$RuCl_3$. The dotted circle in the top view shows the Cl vacancy. In the side view, the magnitudes of the largest displacements along the z direction of each atomic layer are shown in units of Å.

and adjusted through ΔV_0 during the fitting process while the imaginary part V_{im} was fixed at 6 eV. The experimental LEED-*IV* input consists of (00), A and B beams, with incoming electron energy range from 35 to 150 eV. The intensities of C beams are less than 10% of the other beams thus are only used for qualitative comparison rather than input in the fitting process, as shown in figure 3(d).

Before conducting the automated parameter optimization, different layer stacking sequence proposed by Banerjee *et al* [17] and Johnson *et al* [9], were first examined. As expected, different layer stacking sequence has minimum influence on the *IV*-curves in the probed electron energy range, due to limited electron mean free path. The in-plane distortion was also examined by introducing a reasonable atomic displacements (0.2 Å). It turns out that the calculated *IV* curves are also not sensitive to the in-plane displacements that do not give rise to significant intensities in (01) or (10) beam. Furthermore, the in-plane rotational symmetry appears to be intact since the observed diffraction pattern has a clearly 3-fold rotational symmetry. Based on the above calculations and experimental observations, each atom's z coordinates in the unit cell of surface monolayer are allowed for relaxation and the in-plane coordinates are fixed at their bulk values, in the iterative fitting process. The first interlayer distance d is also adjusted.

Best-fit structural parameter values are listed in table 1. The calculated LEED-*IV* curves using optimized structural parameters match well with the experimental curves, as shown in figures 3(a)–(c). However, the dynamical response of (00) beam intensity around 50 eV is not completely captured by theory, due to the energy-independent atomic potential used in the theoretical approximation, which tend to be problematic at lower energies [28–30]. Nevertheless, the evidence of symmetry breaking is best shown in figure 3(d). The calculated (01) and (10) beams intensities are zero across the whole energy range (blue dashed line in figure 3(d)), when assuming an un-distorted $P3_112$ structure. On the other hand, the calculated *IV* curve with optimized distorted coordinates matched well with the experimental curve, in which two main peaks around 40 eV and 55 eV are distinctively present. The optimized results show a strong buckling within the surface monolayer $RuCl_3$. As shown in figure 3(f), the first Cl atomic layer has a buckling, B_{top}, with two Cl atoms (Cl_1, Cl_2) almost at the same plane and third Cl atom (Cl_3) approximately 0.16 Å below. The middle Ru atomic layer has a larger buckling, $B_{Ru} = 0.31$ Å. The bottom Cl atomic layer remains almost flat with a much smaller buckling B_{bottom} of less than 0.03 Å. The total thickness of the surface monolayer is $w' = 2.637$ Å, which is almost unchanged from the unbuckled structure. The determined large buckling in the first Cl atomic layer agreed well with a recent scanning tunneling microscopy (STM) study, where a charge density redistribution with a R_3 super-lattice of the top Cl sub-latice was observed [40]. A unit-cell scale lattice distortion which breaks the inversion symmetry should be considered when constructing the crystal field term in the Hamiltonians for truly 2D

$RuCl_3$. Furthermore, the buckling in the Ru atomic layer induced an extra anisotropy in the two Ru-Ru bond lengths within the unit cell, which is expected to impact the anisotropic Kitaev spin-spin interaction.

4. Origin of the surface monolayer lattice distortion

In order to reveal the nature of buckling, we have carried out first-principles calculations in the framework of density functional theory (DFT) with the projector augmented wave pseudopotential [41, 42] implemented in the Vienna *ab initio* simulation package [43, 44]. The generalized gradient approximation (GGA) in Perdew, Burke and Ernzerhof [45] was used as the exchange-correlation energy and plus Hubbard U method [46] with $U = 2.5$ eV, $J = 0.6$ eV is also applied on Ru(4d) orbitals. The wave functions were expanded in plane waves with an energy cutoff of 600 eV throughout the calculations. The k points were sampled on a Γ-centered 11× 11 mesh in the 2D Brillouin zone of a 1× 1 2D-unit cell containing two Ru atoms and six Cl atoms. Noncollinear magnetic calculations with SOC were included for structure optimizing until the force on each atom was less than 1 meV/Å. Lattice constants obtained by experiments were used in our calculations.

Considering the weak interlayer van der Waals interaction in α-$RuCl_3$, we conducted first-principles calculations on one principal layer (PL), which can give us essential understanding on morphology, electronic and magnetic structures of the surface monolayer. According to the structure optimizing on a 1× 1 2D-lattice containing two Ru atoms, one PL $RuCl_3$ has the symmetry of space group $P\bar{3}1\ m$ with point group D_{3d}. We initially conjectured the electronic origin of the buckling, similar to the Jahn-Teller distortion [47, 48], but the first-principles calculation results do not show any buckling with this consideration. The spin magnetic moment on each Ru atom is almost zero while the orbital moment is 0.44 μ_B. This is the same as the valence electron configuration applied in similar magnetic material system Na_2IrO_3 [49].

To investigate the distortion along z direction, we further expanded the unit cell into a 2× 2 supercell containing eight Ru atoms. Although no distortion happens in defect-free calculation, the displacements the Cl atoms are significant when one Cl vacancy is introduced on the top layer of the supercell, as shown in figure 4(a). The largest displacements along the z direction in the upper and lower layers of Cl and that in the Ru layer are 0.13 Å, 0.22 Å and 0.15 Å, respectively. The buckling of the Cl atoms is consistent with the experimental results of the dynamical LEED-*IV* analysis. The calculation underestimates the value of Ru buckling, which is possibly due to absence of consideration of elevated temperature effects. An important insight gained from this calculation is that Cl atomic defects do have a significant impact on the stability of the lattice and can induce bucklings on *both* Cl and Ru atoms with the same order of magnitude. A combined surface effects due to defects, surface symmetry reduction and interplay between lattice degree of freedom and spin-orbital coupling might be the actual origin of the observed surface intra-layer distortion. Further theoretical and experimental investigations into the origin of the observed distortion are warranted.

5. Conclusions

To summarize, we have deployed combined surface sensitive LEEM and dynamical μ-LEED techniques to study the crystal structure of the surface monolayer of α-$RuCl_3$. We revealed a intra-layer lattice distortion on the surface that breaks the inversion symmetry of previously proposed un-distorted $P3_112$ structure. Both Cl and Ru atoms present significant buckling. The observed distortion is likely induced by surface defects. Considering the spin-orbital coupling effect and a potential emergence of a frustrated quantum spin liquid state at low temperature in α-$RuCl_3$, as well as the observed surface intra-layer distortion presented in this paper, more exotic physics, such as superconductivity [50], may arise from the interplay between lattice degree of freedom and spin-orbital coupling. Furthermore, as a common trait between 2D materials, interlayer interaction is rather weak, similar distortion may also be present in bulk.

Acknowledgment

This research used resources of the Center for Functional Nanomaterials and the National Synchrotron Light Source II, which are U.S. Department of Energy (DOE) Office of Science facilities at Brookhaven National Laboratory, under Contract No. DE-SC0012704. First-principles calculations used the Extreme Science and Engineering Discovery Environment (XSEDE) under Grant No. TG-PHY170023 and Trillian at UNH supported by the NSF MRI program under Grant No. PHY-1229408. J.Z. was supported by the U.S. Department of Energy (DOE), Office of Science, Basic Energy Sciences (BES) under Award No. DE-SC0020221. B.Z. and E.A.H. acknowledge support under NSF DMR-1810305, and from the Institute for Materials Science and Engineering at Washington University in St. Louis. P. L. K. and D. M. were supported by the Gordon and Betty Moore Foundation's EPiQS Initiative Grant No. GBMF4416. J.-Q. Y. acknowledges support from the U.S. Department of Energy (U.S.-DOE), Office of Science - Basic Energy Sciences (BES), Materials Sciences and Engineering Division. We thank Dr. Xiao Tong and Dr. Yuan Huang for useful discussions.

ORCID iDs

Zhongwei Dai https://orcid.org/0000-0001-5450-1060
Samuel A Tenney https://orcid.org/0000-0002-9520-1803
Jiaqiang Yan https://orcid.org/0000-0001-6625-4706
Erik A Henriksen https://orcid.org/0000-0002-4978-2440
Jerzy T Sadowski https://orcid.org/0000-0002-4365-7796

References

[1] Anderson P W 1973 Resonating valence bonds: a new kind of insulator? *Mater. Res. Bull.* **8** 153
[2] Balents L 2010 Spin liquids in frustrated magnets *Nature* **464** 199
[3] Savary L and Balents L 2017 Quantum spin liquids: a review *Rep. Prog. Phys.* **80** 16502
[4] Zhou Y, Kanoda K and Ng T K 2017 Quantum spin liquid states *Rev. Mod. Phys.* **89** 025003
[5] Sarma S D, Freedman M, Nayak C, Modes M Z and 2015 *Npj Quantum Inf.* **1** 15001
[6] Kasahara Y *et al* 2018 Majorana quantization and half-integer thermal quantum hall effect in a Kitaev spin liquid *Nature* **559** 227
[7] Do S H *et al* 2017 Majorana fermions in the Kitaev quantum spin system α-RuCl 3 *Nat. Phys.* **13** 1079
[8] Kitaev A 2006 Anyons in an exactly solved model and beyond *Ann. Phys., NY* **321** 2
[9] Johnson R D *et al* 2015 Monoclinic crystal structure of α-$RuCl_3$ and the zigzag antiferromagnetic ground state *Phys. Rev.* B **92** 235119
[10] Kim B J *et al* 2008 Novel $J_eff = 1/2$ Mott state induced by relativistic spin-orbit coupling in Sr_2IrO_4 *Phys. Rev. Lett.* **101** 076402
[11] Singh Y and Gegenwart P 2010 Antiferromagnetic mott insulating state in single crystals of the honeycomb lattice material Na_2IrO_3 *Phys. Rev.* B **82** 064412
[12] Chaloupka J, Jackeli G and Khaliullin G 2010 Kitaev-heisenberg model on a honeycomb lattice: possible exotic phases in iridium oxides A_2IrO_3 *Phys. Rev. Lett.* **105** 027204
[13] Choi S K *et al* 2012 Spin waves and revised crystal structure of honeycomb Iridate Na_2IrO_3 *Phys. Rev. Lett.* **108** 127204
[14] Lüpke F, Manni S, Erwin S C, Mazin I I, Gegenwart P and Wenderoth M 2015 Highly unconventional surface reconstruction of Na_2IrO_3 with persistent energy gap *Phys. Rev.* B **91** 041405
[15] Sandilands L J, Tian Y, Plumb K W, Kim Y-J and Burch K S 2015 Scattering continuum and possible fractionalized excitations in α-$RuCl_3$ *Phys. Rev. Lett.* **114** 147201
[16] Koitzsch A *et al* 2016 J_eff description of the honeycomb mott insulator α-$RuCl_3$ *Phys. Rev. Lett.* **117** 126403
[17] Banerjee A *et al* 2016 Proximate Kitaev quantum spin liquid behaviour in a honeycomb magnet *Nat. Mater.* **15** 733
[18] Banerjee A *et al* 2017 Neutron scattering in the proximate quantum spin liquid α-$RuCl_3$ *Science* **356** 1055
[19] Cao H B, Banerjee A, Yan J Q, Bridges C A, Lumsden M D, Mandrus D G, Tennant D A, Chakoumakos B C and Nagler S E 2016 Low-temperature crystal and magnetic structure of α-$RuCl_3$ *Physical Review B* **93** 134423
[20] Sinn S *et al* 2016 Electronic structure of the Kitaev material α-$RuCl_3$ probed by photoemission and inverse photoemission spectroscopies *Sci. Rep.* **6** 39544
[21] Zhou X *et al* 2016 Angle-resolved photoemission study of the Kitaev candidate α-$RuCl_3$ *Phys. Rev.* B **94** 161106
[22] Zhou B, Wang Y, Osterhoudt G B, Lampen-Kelley P, Mandrus D, He R, Burch K S and Henriksen E A 2018a Possible structural transformation and enhanced magnetic fluctuations in exfoliated α-$RuCl_3$ *J. Phys. Chem. Solids* **128** 291
[23] Du L *et al* 2019 2D proximate quantum spin liquid state in atomic-thin α-$RuCl_3$ *2D Mater.* **6** 015014
[24] Zhou B, Balgley J, Lampen-Kelley P, Yan J Q, Mandrus D G and Henriksen E A 2018 Gate-tuned charge-doping and magnetism in graphene/α-$RuCl_3$ heterostructures *Phys. Rev.* B **100** 165426
[25] Mashhadi S *et al* 2019 Spin-split band hybridization in graphene proximitized with α-$RuCl_3$ nanosheets *Nano Lett.* **19** 4659
[26] Bauer E 2014 *Surface Microscopy with Low Energy Electrons* (New York: Springer) (https://doi.org/10.1007/978-1-4939-0935-3)
[27] Adams D L 2002 A simple and effective procedure for the refinement of surface structure in LEED *Surf. Sci* **519** 157
[28] Pendry J B 1974 *Low-Energy Electron Diffraction* (London: Academic) (https://doi.org/10.1007/978-1-4684-8777-0_7)
[29] van Hove M and Tong S Y 1979 *Surface Crystallography by Leed* (Berlin: Springer) (https://doi.org/10.1007/978-3-642-67195-1)
[30] Sun J, Hannon J B, Kellogg G L and Pohl K 2007 Local structural and compositional determination via electron scattering: Heterogeneous Cu(001)-Pd surface alloy *Phys. Rev.* B **76** 205414
[31] Dai Z *et al* 2017 Surface buckling of black phosphorus: Determination, origin and influence on electronic structure *Phys. Rev. Mater.* **1** 074003
[32] Jin W *et al* 2013 Direct measurement of the thickness-dependent electronic band structure of MoS_2 using angle-resolved photoemission spectroscopy *Phys. Rev. Lett.* **111** 106801
[33] Jin W *et al* 2015 Substrate interactions with suspended and supported monolayer MoS_2: Angle-resolved photoemission spectroscopy *Phys. Rev.* B **91** 121409
[34] Lander J J and Morrison J 1963 Structures of clean surfaces of Germanium and Silicon I *J. Appl. Phys.* **34** 1403
[35] Tosatti E and Anderson P W 1974 Two-dimensional excitonic insulators: Si and Ge (111) surfaces *Solid State Commun.* **14** 773
[36] Koitzsch A *et al* 2017 Nearest-neighbor Kitaev exchange blocked by charge order in electron-doped α-$RuCl_3$ *Phys. Rev. Mater.* **1** 052001
[37] Kong T, Stolze K, Timmons E I, Tao J, Ni D, Guo S, Yang Z, Prozorov R and Cava R J 2019 Ferromagnetic semiconductors: VI_3—a new layered ferromagnetic semiconductor *Adv. Mater.* **31** 1970126
[38] Zangwill A 1988 *Physics at Surfaces* (Cambridge: Cambridge University Press) (https://doi.org/10.1017/CBO9780511622564)
[39] https://www.icts.hkbu.edu.hk/vanhove/VanHove_files/leed/leedpack.html
[40] Ziatdinov M *et al* 2016 Atomic-scale observation of structural and electronic orders in the layered compound α-$RuCl_3$ *Nat. Commun.* **7** 13774
[41] Blöchl P E 1994 Projector augmented-wave method *Phys. Rev.* B **50** 17953
[42] Kresse G and Joubert D 1999 From ultrasoft pseudopotentials to the projector augmented-wave method *Phys. Rev.* B **59** 1758
[43] Kresse G and Furthmüller J 1996a Efficiency of ab-initio total energy calculations for metals and semiconductors using a plane-wave basis set *Comput. Mater. Sci.* **6** 15
[44] Kresse G and Furthmüller J 1996b Efficient iterative schemes for ab initio total-energy calculations using a plane-wave basis set *Phys. Rev.* B **54** 11169

[45] Perdew J P, Burke K and Ernzerhof M 1996 Generalized gradient approximation made simple *Phys. Rev. Lett.* **77** 3865
[46] Liechtenstein A I, Anisimov V I and Zaanen J 1995 Density-functional theory and strong interactions: Orbital ordering in Mott-Hubbard insulators *Phys. Rev.* B **52** R5467
[47] Jahn H A and Teller E 1937 Stability of polyatomic molecules in degenerate electronic states - I: Orbital degeneracy *Proc. R. Soc. Lond.* A **161** 220
[48] Jahn H A and Teller E 1938 Stability of polyatomic molecules in degenerate electronic states - II: Spin degeneracy *Proc. R. Soc. Lond.* A **164** 117
[49] Jackeli G and Khaliullin G 2009 Mott Insulators in the Strong Spin-Orbit Coupling Limit: From Heisenberg to a Quantum Compass and Kitaev Models *Phys. Rev. Lett.* **102** 017205
[50] Wang B B, Wang W, Yu S L and Li J X 2019 Particle-hole fluctuations and possible superconductivity in doped α-$RuCl_3$ *Chinese Phys.* B **28** 057402